International Journal of Nanoelectronics and Materials
IJNeaM
ISSN 1985-5761 | E-ISSN 2232-1535

Graphitic carbon nitride/ zinc oxide heterostructure photocatalyst for Azo dye removal and electricity generation via photocatalytic fuel cell

Jai-Xien OrYang [a,b], Li-Ngee Ho [a,b] *, Chang-Chuan Lee [c], Kang-Zheng Khor [a,d], and Soon-An Ong [b,e]

[a]*Faculty of Chemical Engineering & Technology, Universiti Malaysia Perlis, 02600 Arau, Perlis, Malaysia*
[b]*Water Research and Environmental Sustainability Growth, Centre of Excellence, Universiti Malaysia Perlis, 02600 Arau, Perlis, Malaysia*
[c]*Faculty of Mechanical Engineering & Technology, Universiti Malaysia Perlis, Perlis, Malaysia*
[d]*Frontier Materials Research, Centre of Excellence, Universiti Malaysia Perlis, Perlis, Malaysia*
[e]*Faculty of Civil Engineering & Technology, Universiti Malaysia Perlis, 02600 Arau, Perlis, Malaysia*
** Corresponding author. e-mail: lnho@unimap.edu.my, holingee@yahoo.com*

Received 8 December 2024, Revised 20 December 2024, Accepted 25 December 2024

ABSTRACT

Photoanode is a crucial part of the photocatalytic fuel cell (PFC) system because of its function in degrading organic pollutants and producing electrons for electricity generation. A facile way was used to fabricate the heterojunction graphitic carbon nitride/zinc oxide (GCN/ZnO) composites through the combustion of urea and zinc acetate dihydrate in three different mass ratios. The synthesised GCN/ZnO composites were then loaded on a carbon plate as a photoanode by employing ultrasonication and immobilisation methods. The synthesised GCN/ZnO composites were characterised by using X-ray diffraction (XRD), Fourier-transformed infrared spectroscopy (FTIR), N_2 sorption–desorption isotherms and scanning electron microscopy (SEM). The GCN/ZnO photoanode was applied in a PFC with platinum-loaded carbon paper as the cathode. Reactive Red 120 (RR120) was used as a model pollutant in the PFC under ultraviolet light (UVA) irradiation. The findings revealed that the GCN/ZnO2 heterojunction photoanode achieved a decolourisation efficiency of 55.24% in 10 mg/L of RR120, which was 0.9 times higher than that of the GCN photoanode, while the maximum power density was 17.14 mW/m^2, which was 13.39 times compared with that of the GCN photoanode.

Keywords: *Graphitic carbon nitride, Zinc oxide, Photocatalytic fuel cell, Heterojunction, Band gap*

1. INTRODUCTION

The problem of water pollution has grown into a worldwide concern due to the fast pace of urban development. Discharging dyes into water sources contributes to contamination issues as dye processes have led to the yearly wastage of around 200,000 tons of dye as effluents [1]. Contaminated water with dyes has an adverse impact on the environment. High dye load in those effluents inhibit aquatic photosynthesis of plants and organisms under the water due to limited light transmission [2]. It not only degrades the visual appeal of water bodies but also raises the levels of biochemical and chemical oxygen demand. As a result, the dye-polluted water can endanger aquatic life [3]. Therefore, it is essential to develop an effective and sustainable wastewater treatment process to address water pollution and ensure the well-being of future generations. This effort aligns with the Sustainable Development Goals (SDGs), specifically Goal 6: Clean Water and Sanitation, and Goal 14: Life Below Water.

Photocatalytic fuel cells (PFC) are gaining popularity as a viable technique for wastewater treatment and electricity production concurrently [4]. It utilises light energy to activate photocatalysts on the surface of the photoanode, generating electron-hole pairs that drive redox reactions for pollutant degradation and electricity generation. The effectiveness of PFC is mostly determined by the photocatalyst utilised at the anode or cathode, which should be photoactive, stable, and capable of absorbing visible light [5].

Recently, graphitic carbon nitride (GCN) has become increasingly attractive as a low-cost and benign semiconductor material due to its environmentally friendly and sustainable benefits. The resilience to abrasive environments and appropriate energy band edges promote GCN a favour for chemical transformation processes like water splitting [6]. Unlike general semiconductor materials such as metal oxide, GCN is a metal-free material that can easily be accessed from carbon-based materials, such as thiourea, melamine, urea, etc [7]. Many studies show that GCN exhibits as a good photocatalyst for wastewater treatment, and various methods are applied to synthesise GCN from different precursors, for example, the direct growth method [8], chemical vapour deposition [9] and template-assisted synthesis [10], however, these methods are time-consuming and costly. Furthermore, researchers soon found that using GCN as a photocatalyst encountered issues with the rapid recombination of photogenerated electron holes and narrow light absorption range which reduced the overall photocatalytic activities [11]. Consequently, the idea of synthesising GCN with metal oxide heterojunction material is believed to improve the

photocatalytic activity of GCN by altering its band gap via a facile method.

Zinc oxide (ZnO) has a broad direct band gap of around 3.37 eV, allowing it to absorb a large amount of UV and visible light spectrum [12]. This feature makes it suitable for photocatalytic applications since it can efficiently create electron-hole pairs under light irradiation. Furthermore, ZnO has high electron mobility, aiding the fast transfer of charge carriers, which is critical for improving photocatalytic activity and overall efficiency in energy conversion processes [13]. It is believed that the combination of ZnO with GCN can widen the band gap of GCN and solve the problem of rapid charge recombination while improving its photocatalytic activity.

In this study, we explored a facile method for producing GCN/ZnO photoanode for application in PFC. The band gap of the GCN was altered by incorporating varying amounts of zinc acetate into the urea during synthesis to form GCN/ZnOγ composites, aiming to evaluate the influence of GCN/ZnO composites at various ratios on the decolourisation efficiency and electricity generation in the PFC.

2. MATERIALS AND METHODS

2.1. Materials and Chemicals

The organic pollutant used in this study was azo dye Reactive Red 120 (RR120) ($C_{44}H_{30}Cl_2N_{14}O_{20}S_6$) provided by Sigma Aldrich. Urea ($CO(NH_2)_2$) with a molecular weight of 60.06 g/mol was purchased from Bendosen and used as the precursor of GCN. Meanwhile, zinc acetate dihydrate ($Zn(CH_3CO_2)_2{\cdot}2H_2O$) with a molecular weight: 219.51 g/mol supplied by Riedel was used to synthesise ZnO. The following chemicals were purchased from HmbG Chemicals: ethanol (C_2H_5OH, 95%) was used to clean photoanodes, ethylene glycol ($C_2H_6O_2$) was used in the fabrication of photoanode, and sodium sulphate (Na_2SO_4) was applied as the supporting electrolyte in the study. All the chemicals employed were of analytical grade with no further purification.

2.2. Synthesis of GCN

An alumina crucible (50 mL) with 20 g of urea was heated in the muffle furnace to 520°C with a heating rate of 3°C/min for 3 hours. Ultimately, the sample was ground in the mortar to attain a fine powder of GCN.

2.3. Synthesis of GCN/ZnOγ Heterostructures Composites

GCN/ZnOγ composites were prepared in different zinc acetate dihydrate amounts with a fixed amount of urea (refer to Table 1) using the calcination method. An alumina crucible (50 mL) with 20 g of urea and 1 g of zinc acetate was weighed and mixed homogeneously before being heated in the muffle furnace to 520°C, with a heating rate of 3°C/min for 3 hours. Finally, the sample was ground in the mortar to attain a fine powder of GCN/ZnO1. Similarly, GCN/ZnO2 and GCN/ZnO3 hybrid materials were produced by adjusting the quantity of zinc acetate to 2 and 3 g while maintaining a consistent amount of urea (20 g) and keeping all other conditions unchanged.

Table 1. Amount of urea and zinc acetate for synthesis of GCN/ZnOγ composites

Sample	Mass of urea (g)	Mass of zinc acetate dihydrate (g)
GCN/ZnO1	20.00	1.00
GCN/ZnO2	20.00	2.00
GCN/ZnO3	20.00	3.00

2.4. Preparation of Photoanode

A carbon plate as the substrate of the photoanode was prepared in the dimensions of 30 × 30 × 10 mm. Ultrasonic cleaning of the carbon plate with deionised water and ethanol was accomplished in an ultrasonic bath. The suspension of GCN was formulated by dispersing 0.4 g of GCN powder with a proper ratio of ethylene glycol and deionised water. Next, the carbon plate was immobilised with the GCN suspension. The GCN-loaded carbon plate (GCN/C) was dried in the oven at 60°C for 2 hours and transferred to the muffle furnace at 80°C for 10 minutes for heat treatment. Three different photoanode types were prepared: GCN/ZnO1, GCN/ZnO2 and GCN/ZnO3 using the same method.

2.5. PFC Setup and Operation

The PFC was assembled with platinum-loaded carbon (Pt/C) paper as a cathode and photoanodes in a 600 mL beaker filled with 250 mL of 10 mg/L of RR120. The cathode and photoanode were connected via a circuit with a resistance of 1000 Ω. The distance between the two electrodes was 30 mm. The Ultraviolet-A (UVA) lamp and the photoanode were set up with a distance of 50 mm, the UVA lamp was purchased from Philips rated at 7.7 W and emitting light at 350 to 400 nm. Then the reactor was agitated by a magnetic stirrer and air bubbles were introduced at a flow rate of 0.4 L/min using an airflow meter (Model: LZB-3, China). The PFC was conducted at room temperature for 6 hours of reaction time.

2.6. Materials Characterisation

X-ray diffraction (XRD) was used to analyse the crystal structure and the phase compositions of the samples. The instrument used was a Bruker D2 Phaser model with Cu-Kα radiation (λ = 1.54184 Å). The XRD data was gathered by scanning from 2θ = 5˚ to 80˚ at a scan rate of 0.1 s/step. The functional groups in the synthesised samples were examined by a Fourier transform infrared spectrometer (FTIR) from Perkin Elmer (Model: Spectrum RX1 Spectrometer). The morphology and microstructure of the samples were observed by utilising scanning electron microscopy (SEM) with energy-dispersive X-ray spectroscopy (EDX) from JEOL (Model: JSM-6460LA). The

specific surface areas of the synthesised samples were measured from N_2 sorption–desorption isotherms at 77 K with an instrument from (Micromeritics, TriStar 3000 V6.06A) based on Brunauer–Emmett–Teller (BET) equation. The ultraviolet-visible diffuse reflectance spectra (UV-Vis DRS) were examined by an ultraviolet-visible (UV-Vis) spectrophotometer from Agilent (Model: Cary 100). For the band gap (E_g) calculation, the photon energy equation was used as the following Equation (1):

$$E_g = \frac{hc}{\lambda} \quad (1)$$

2.7. Measurement and Analysis of Electricity Generation in PFC

During the polarization test, the cell voltage across the 1000 Ω external resistors was measured and recorded every hour using a digital multimeter (Model: CD800a from Sanwa Electric Instrument, Japan) as the resistor varied from 1 MΩ to 10 Ω. The power density (P, mW/cm^2) of the PFC was calculated by the following Equation (2):

$$P = \frac{VI}{A} \quad (2)$$

where V is the PFC's voltage output (mV), I is the current (mA), and A is the area of the photoanode.

2.8. Measurement of Decolourisation in PFC

UV-Vis spectroscopy (Model: ME-UV1300 PC from Mesulab, China) was utilised to determine the RR120 concentration at λ_{max} = 536 nm. The water sample was taken and examined every 1 hour of the reaction time. The colour removal efficiency was calculated by applying Equation (3):

$$CR_E = \frac{C_0 - C_t}{C_0} \times 100 \quad (3)$$

where C_0 is the initial dye concentration and C_t is the dye concentration at a specified reaction time, t (h).

The dye decolourisation rate was simulated using the pseudo-first-order kinetics. The first-order decolourisation kinetics constant (k) was assessed based on Equation (4):

$$ln\left(\frac{C_0}{C_t}\right) = kt \quad (4)$$

where k is the slope from the plot of ln (C_0/C_t) against time (t).

3. RESULTS AND DISCUSSION

3.1. Materials Characterisation

3.1.1. Phase Analysis

As depicted in Figure 1, X-ray diffraction (XRD) patterns of GCN and GCN/ZnO1 revealed a prominent peak at

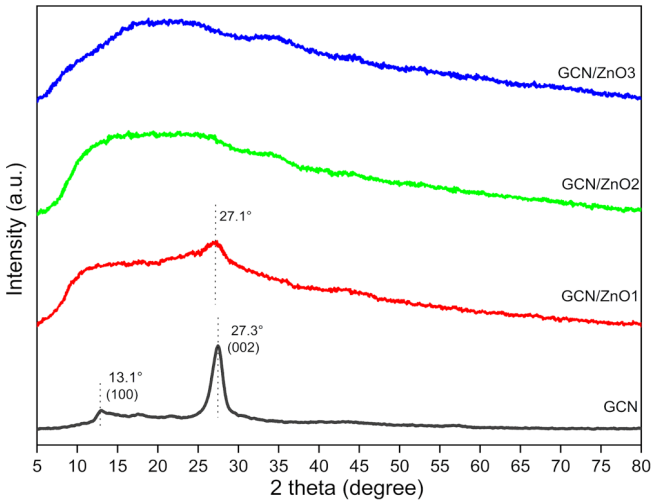

Figure 1. XRD patterns of GCN and synthesised GCN/ZnOγ composites

2θ = 27.3° and 27.1° respectively, indicating the presence of the (002) plane. This disclosed the interlayer C–N stacking of conjugated aromatic systems in GCN and GCN/ZnO1 in agreement with the crystal structures of pure GCN (JCPDS card 87-1526) [14]. This main peak slightly shifted to 0.2° lower (27.1°) in GCN/ZnO1 compared to that of the pure GCN (27.3°) due to the expansion of interlayer stacking spacing which might be attributed to the introduction of ZnO into the graphitic carbon nitride structure [15]. Besides, a lower peak also showed up at 13.1° in GCN, representing the (100) plane and could be attributed to the periodic arrangement of s-triazine units [14]. The hole-to-hole distance of nitride pores in the in-plane structural packing motif in GCN caused the 100 planes to occur [16]. Moreover, while the content of zinc acetate dihydrate in the precursor system rose, the intensity of the (002) and (100) peaks were found to slightly shift and decline. This suggested that the presence of ZnO was found to inhibit the growth of GCN crystal in the graphitic carbon nitride structure resulting in distortion of the nitride pore structure and changing the hole-to-hole distance, respectively [16, 17]. Furthermore, the ZnO peak was not observed in all the XRD patterns of the GCN/ZnOγ samples where only an amorphous phase was seen. The reason could be the small quantity of ZnO in GCN/ZnOγ composites [16, 18].

3.1.2. Chemical Compound and Functional Group Analysis

As shown in Figure 2, the FTIR spectrum declared C and N bonding in GCN and GCN/ZnOγ composites. In GCN/ZnOγ composites, the peak at 525 cm^{-1} could be assigned to Zn–O bonding, however, the intensity of the peak being broad and less significant, and the development of a new C=O bond at peak ~ 2167 cm^{-1} took place and was noticed to be getting more intense with rising $Zn(CH_3CO_2)_2{\cdot}2H_2O$ content which similar as the finding of Paul *et al.* [16], this might be due to the existence of CO_2 molecules in the atmosphere when the combustion of GCN/ZnOγ composites [19]. In GCN, it was found a sharp peak at 808 cm^{-1} corresponding to the breathing mode of the s-triazine ring. On the other hand, the

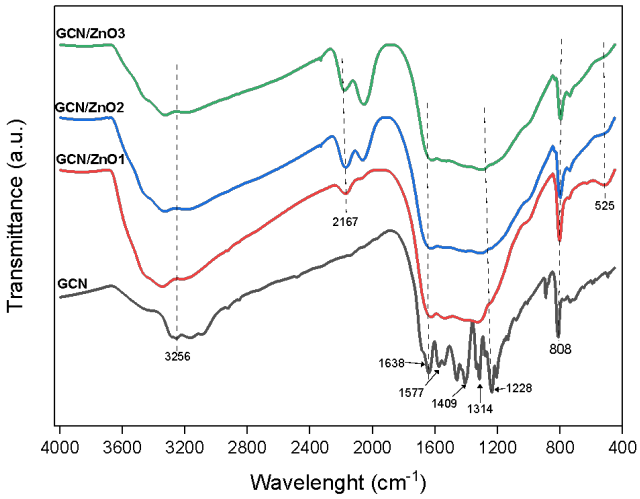

Figure 2. FTIR spectra of GCN and GCN/ZnOγ composites

peaks were found to be slightly shifted to 801, 798, and 796 cm^{-1} in GCN/ZnO1, GCN/ZnO2 and GCN/ZnO3 due to the lower conjugation of GCN and ZnO in the composite [14]. The peaks around 1228, 1314, and 1409 cm^{-1} were associated with the C–N stretching vibration such as C–NH–C and C–N(–C)–C units, meanwhile, the other two peaks around 1577 and 1638 cm^{-1} could be assigned to the C=N stretching vibration in GCN and GCN/ZnOγ composites [20, 21]. These peaks significantly became broader when the amount of Zn $(CH_3CO_2)_2{\cdot}_2H_2O$ increased. This phenomenon could be due to the addition of ZnO into the GCN giving rise to the extension of the C_3N_4 arrangement [14, 16]. In GCN and GCN/ZnOγ composites, the broad peaks between 3090 and 3500 cm^{-1} originated from the N–H stretching vibrations of peripheral amino groups along with the O–H stretching vibrations of surface hydroxyl groups were observed. However, introducing oxygen functionalities could account for broader peaks in GCN/ZnO composites [22].

3.1.3. Morphology and Microstructure Analysis

The morphology of the GCN and GCN/ZnOγ composite was examined by SEM under different magnifications. The GCN in Figure 3 (a) showed irregularly stacked foil-like layered nanostructures [21]. When ZnO was introduced to the GCN, the abundant nanoparticles of ZnO were attached and dispersed on the surface of a graphitic carbon nitride sheet-like structure as could be observed in Figures 3 (c) & (d), (e) & (f) and (g) & (h) [21, 23]. This occurrence revealed that the introduction of ZnO to GCN could alter the microstructure of the original graphitic carbon nitride, which correlated to the findings of XRD analysis. From qualitative analysis, it was evident that the synthesised GCN/ZnOγ composites consisted of zinc (Zn), oxygen (O), carbon (C) and nitrogen (N) elements as attested in the EDX analysis in Figure SM-1 to SM-3.

3.1.4. Surface Area and Pore Properties Analysis

The synthesised GCN and GCN/ZnOγ composites depicted type IV isotherms with H3 hysteresis loop, as shown in Figures SM-4 (a) to (d). These results suggested that the

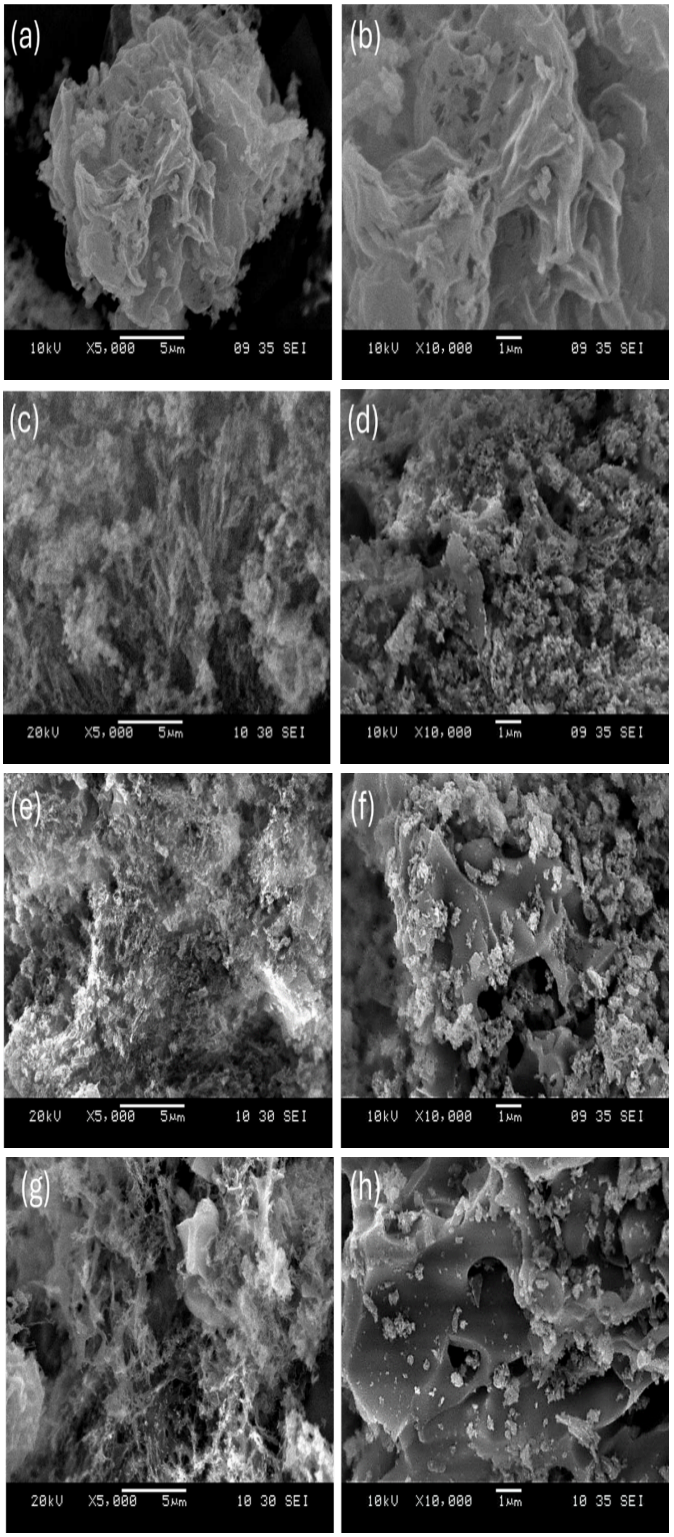

Figure 3. SEM images of (a) & (b) GCN, (c) & (d) GCN/ZnO1, (e) & (f) GCN/ZnO2, and (g) & (h) GCN/ZnO3 composites

samples displayed slit-shaped pore structures in the resultant composite [24–26]. The hysteresis loops filled at high relative pressures (P/P_0) in the range of 0.6 to 1.0, indicating the presence of mesopores and macropores within the structure [27] and these were confirmed by the pore size distribution analysis as shown in Figure SM-5 which proved that the samples contained both macropores and mesopores, with the majority of the pore size falling under the range of around 15–80 nm [28].

Table 2 presented the BET surface area and total pore volume of the synthesised GCN and GCN/ZnOγ composites, it depicted a decreasing trend in both surface area and the total pore volume following the order of GCN > GCN/ZnO1 > GCN/ZnO2 > GCN/ZnO3, as the zinc acetate dihydrate content increased. This was likely due to ZnO particles filling up the pores of GCN, inhibiting the formation of a regular nanosheet layer structure, as observed in the SEM (Figure 3 (c)–(h)), which in turn reduced the BET surface area and the total pore volume of the GCN/ZnOγ composites. Notably, the surface area of GCN/ZnO3 (5 m^2/g) was 13.4 times smaller than that of GCN (66 m^2/g), while the total pore volume of GCN was almost 12 times greater than GCN/ZnO3.

3.1.5. Band Gap Analysis

The band gap of the GCN and GCN/ZnOγ composites was analysed by using UV-Vis DRS as revealed in Figure 4. All the samples were analysed in the range of UV (200 nm) to visible light up to 700 nm. The primary absorption edge of the GCN was at 448 nm. When GCN combined with ZnO, the absorption edge of GCN/ZnOγ composites shifted notably to a longer wavelength and more robust absorption than GCN in the visible light range from 500–700 nm. Apparently, the absorbance increased gradually when ZnO was added to the GCN structure. Meanwhile, GCN/ZnO2 and GCN/ZnO3 possessed similar absorption capabilities around 350–400 nm, yet GCN/ZnO2 showed slightly higher absorption capacity around 360–390 nm and strongest absorbance especially in the visible range of 450–700 nm compared to GCN/ZnO3. The results indicated that GCN/ZnO2 possessed the highest light-harvesting properties, which could enhance photo-excited e^-/h^+ pairs production, thus helping to lift the photocatalytic activity efficiency compared to other samples in this study [29]. The band gap energy (E_g) of the samples was estimated based on the photon energy equation. The E_g value of the samples was approximately 2.74 eV (GCN), 2.49 eV (GCN/ZnO1), 2.25 eV (GCN/ZnO2) and 2.31 eV (GCN/ZnO3), respectively. It is noticed that the introduction of ZnO into the GCN could narrow the band gap of the synthesised materials causing an enrichment of photo sorption capability which was similar to the finding of Navidpour *et al.* [30]. The reducing band gap observed in GCN/ZnO3 could be attributed to the quantum confinement effect in the smaller crystal size, this is because the ZnO formation inhibited the crystal growth of GCN when increased the amount of zinc acetate dihydrate to GCN during the synthesis process [31].

3.2. Effect of GCN and GCN/ZnOγ Composites as Photoanode on RR120 Dye Removal Efficiency in PFC

As shown in Figure 5 (a), all the colour removal efficiencies of PFCs with different types of photoanodes depicted upward trends. The degradation efficiency of the GCN and GCN/ZnOγ composites loaded on the carbon plate for RR120 treatment depleted the following the order of GCN/ZnO2 > GCN/ZnO1 > GCN > GCN/ZnO3. The colour removal efficiency of RR120 was 47.87% after 6 hours by using GCN/C as a photoanode, while the decolourisation

Table 2. Specific surface area (S_{BET}), pore diameter (D_p) and total pore volume (V_p) of GCN and GCN/ZnOγ samples

Sample	S_{BET} (m^2 g^{-1})	D_p (nm)	V_p (cm^3 g^{-1})
GCN	67	10.7	0.1802
GCN/ZnO1	27	10.3	0.0697
GCN/ZnO2	11	9.9	0.0282
GCN/ZnO3	5	11.3	0.0154

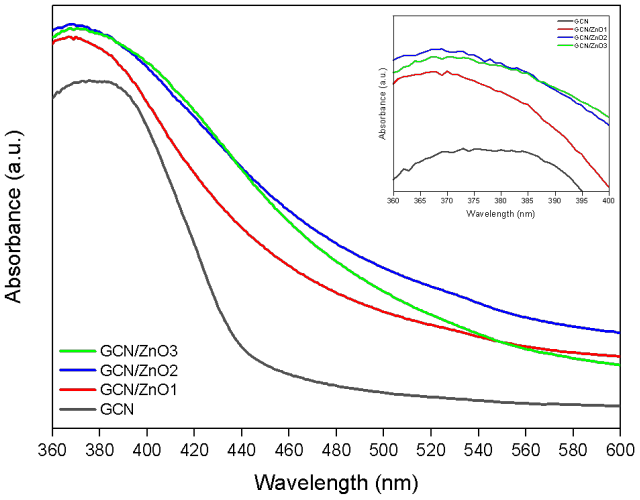

Figure 4. UV-Vis diffuse spectrum of synthesised GCN, GCN/ZnO1, GCN/ZnO2 and GCN/ZnO3

efficiency of using GCN/ZnO2 as a photoanode was 55.24% under the same condition. Although a larger surface area often correlates with enhanced degradation efficiency [32–35]. It was interesting to find that the colour removal efficiency was not mainly dependent on the surface area of the samples as demonstrated in Table 2, as GCN/ZnO2 with the second-smallest surface area, exhibited the highest colour removal efficiency. The improved performance of GCN/ZnO2 can be attributed to its unique photocatalytic properties. Its smallest band gap of 2.25 eV compared to other synthesised composites, exhibited the highest light adsorption capability around 360–390 nm in the wavelength of UVA light facilitating it to absorb more light energy for electron-hole pair generation and subsequent RR120 degradation. The improvement of degradation efficiency could be affected by the photocatalytic properties of the samples, which could be attributed to the presence of ZnO in the hybrid composites. However, the degradation efficiency of the colour did not improve further when the quantity of zinc acetate increased above GCN/ZnO2, as perceived in the colour removal efficiency of GCN/ZnO3/C as a photoanode dropped to 41.03% which was lower than that of GCN (47.87%) at 6 h under UVA light irradiation condition. This phenomenon revealed that there was a synergetic effect between GCN and ZnO for improving the colour degradation efficiency by reducing the band gap energy from 2.74 eV (GCN) to 2.25 eV (GCN/ZnO2), however, an extra amount of ZnO in the GCN/ZnO3 surged the recombination site in electron hole-pair which then inhibited the transfer frequency of photo-induced charge [16].

The kinetic rate constant was calculated according to pseudo-first-order kinetics using the Langmuir-Hinshelwood model, as shown in Figure 5 (b). GCN/ZnO2 exhibited the highest value for the apparent rate constant (0.1324 h^{-1}) resulting in an increment of 1.23 times in comparison to that of GCN (0.10759 h^{-1}), as demonstrated in Table 3, while GCN/ZnO3 with 0.08559 h^{-1} showed the lowest apparent rate constant among the photoanodes. This result was in agreement with the results of decolourisation efficiency of RR 120 as depicted in Figure 5 (a). Hence, the photocatalytic activity had a linear relationship with the colour removal efficiency. This finding was also compatible with the results of Lee *et al.* [36] in the study of photodegradation of different dyes in PFC.

Table 3. Pseudo-first order apparent rate constant, k_{app} (h^{-1}) for different photoanodes

Photoanode	Apparent rate constant, k_{app} (h^{-1})	Goodness-of-fit, R^2
GCN	0.10759	0.99843
GCN/ZnO1	0.1232	0.99607
GCN/ZnO2	0.1324	0.99824
GCN/ZnO3	0.08559	0.99664

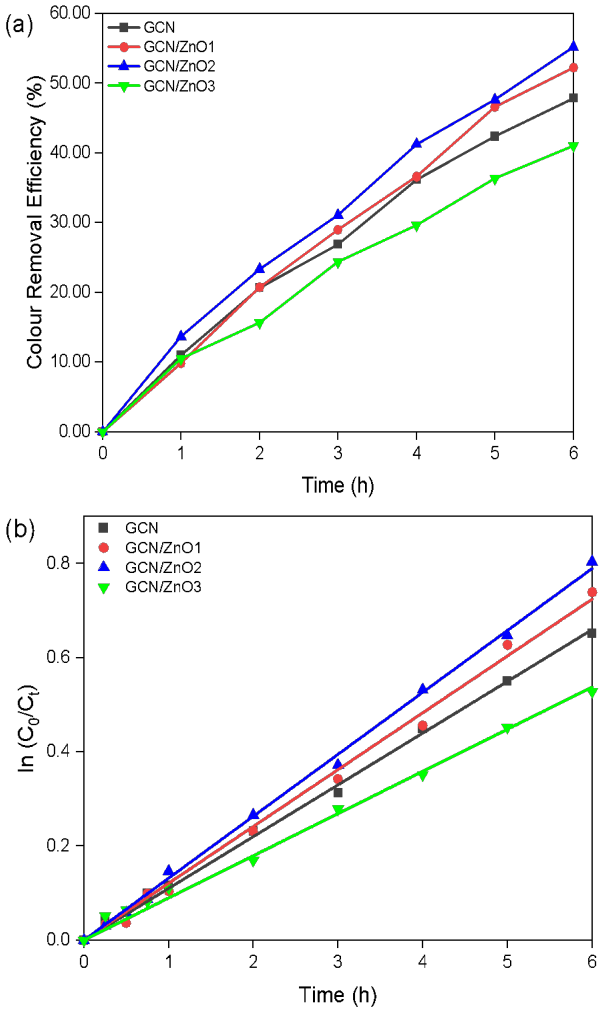

Figure 5. Colour removal efficiency and (b) Kinetic photocatalytic degradation of PFC with various photoanodes in 10 mg L^{-1} of RR120 over 6 hours irradiation time under UVA light irradiation

3.3. Effect of GCN and GCN/ZnOγ Composites as Photoanodes on the Electricity Generation in PFC

The effects of the different photoanodes were significant on the electricity generation in the PFC as seen in Figure 6 (a). Generally, the trend of the voltage output of GCN and GCN/ZnOγ composites as photoanodes was similar to the trend of the decolourisation efficiency. GCN/ZnO2 photoanode yielded the highest voltage output (146.1 mV) while the voltage output of GCN/ZnO3 photoanode only generated less than 16.4 mV at the end of 6 h reaction time. A significant disparity was observed between GCN/ZnO2 and GCN/ZnO3 as photoanode: a 29% difference in degradation efficiency and a substantial 159% difference in voltage output. These discrepancies can be attributed to variations in surface area and pore volume of the synthesised photocatalysts. GCN/ZnO3, with its lower pore volume and smaller BET surface area compared to GCN/ZnO2, exhibits reduced light adsorption and catalytic activity, hindering electron mobility [37, 38]. Furthermore, GCN/ZnO3 displayed the lowest reaction kinetic rate in degradation efficiency RR120 among the synthesised photoanodes. The low rate of reaction kinetic could slow down the photoexcited electron separation and holes idle on the photocatalyst surface for longer periods, which may result in an accumulation of charge carriers on the surface, increasing the likelihood of recombination [39]. As the formation of photogenerated holes on the surface of the catalyst reduced, the colour removal efficiency declined, resulting in the downturn of •OH radicals formation, thus resulting in a reduction or saturation on electrons formation to transport to the cathode via external circuit, finally producing low voltage output [40]. Consequently, it could be concluded that there was a linear relationship between the decolourisation efficiency and the voltage output of the PFC in this study.

Figures 6 (b) and (c) illustrate the polarisation curves and power density curves of PFC systems under UVA light irradiation with various photoanodes. The voltage open circuit (V_{oc}), short circuit current density (J_{sc}) and maximum power density (P_{max}) in the PFC with different photoanodes decreased in the order of: GCN/ZnO2 > GCN/ZnO1 > GCN > GCN/ZnO3. Specifically, GCN/ZnO2 showed the highest V_{oc} at 328.8 mV, which was a factor of 1.43 compared with GCN alone (229.4 mV). Additionally, the PFC performance using GCN/ZnO2 as photoanode showed a substantial increase in J_{sc} and P_{max}, reaching 237.04 mA/m^2 and 17.14 mW/m^2, respectively, compared to 28.39 mA/m^2 and 1.28 mW/m^2 in the PFC with GCN as photoanode. On the other hand, the lowest V_{oc}, J_{sc}, and P_{max} values were recorded in the PFC with GCN/ZnO3 as the photoanode with 166.5 mV, 12.83 mA/m^2 and 0.34 mW/m^2, respectively. The highest performance in V_{oc}, J_{sc} and P_{max} of GCN/ZnO2 illustrates that efficient charge separation caused by heterojunctions in the GCN/ZnO composite results in the participation of more photogenerated carriers. In contrast, further increasing the amount of ZnO up to GCN induced significant particle agglomeration and thereby enhanced the recombination rate of electrons and holes, consequently lowering the photocatalytic efficiency as could be observed in GCN/ZnO3

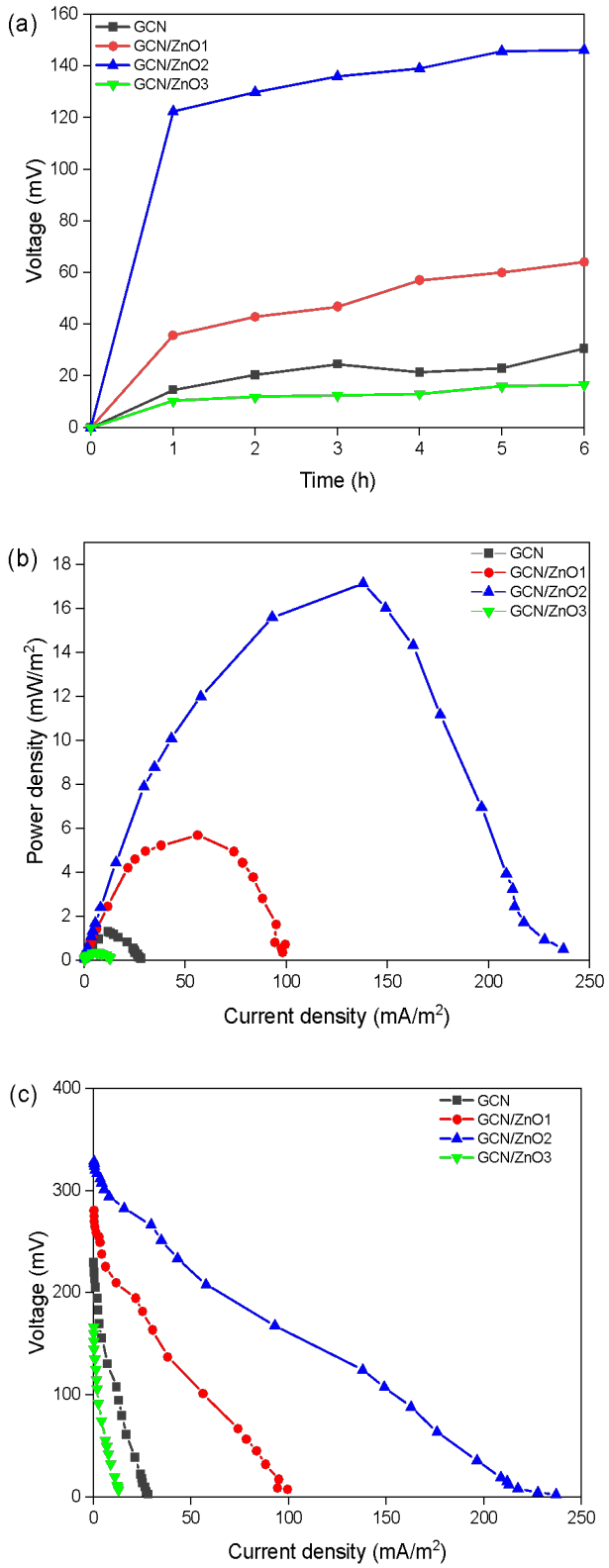

Figure 6. (a) Voltage output (b) Power density curves and (c) Polarisation curves with different photoanodes under UVA light irradiation

[37, 41]. This indicated an appropriate amount of ZnO to GCN was important in influencing the rate of electron transfer in GCN/ZnO photoanode [42]. Overall, the results of the maximum power density, short circuit current density and open circuit voltage were compatible with the sequence of the colour removal efficiency.

4. CONCLUSION

In summary, GCN/ZnO composite photoanodes were successfully fabricated and applied in a PFC with Pt/C paper as a cathode. The maximum voltage open circuit was 1.43 times higher in the PFC with GCN/ZnO2 photoanode (328.8 mV) than that of the GCN photoanode (229.4 mV). The kinetic photocatalytic decolourisation of RR120 in the PFC increased in the order of GCN/ZnO3 < GCN < GCNZnO1 < GCN/ZnO2. The enhanced performance in the PFC using GCN/ZnO composites as photoanodes could be attributed to the heterojunction in the GCN/ZnO and the improved ability of the charge interface carrier separation. Lastly, the heterostructures formed between GCN and ZnO showed a synergetic effect which improved both the transfer efficiency of photogenerated electron-hole pairs and the redox capability. This study provided important insights for the synthesis and modification of GCN/ZnO composite for application as the photoanode in PFC to degrade azo dye and generate electricity synchronously.

ACKNOWLEDGMENTS

This research was supported by the Fundamental Research Grant Scheme (FRGS/1/2022/STG05/UNIMAP/02/1) provided by the Ministry of Higher Education, Malaysia.

REFERENCES

[1] F. M. Drumond Chequer, G. A. R. de Oliveira, E. R. Anastacio Ferraz, J. Carvalho, M. V. Boldrin Zanoni, and D. P. de Oliveir, "Textile Dyes: Dyeing Process and Environmental Impact," in *Eco-Friendly Textile Dyeing and Finishing*, InTech, 2013. doi: 10.5772/53659.

[2] S. Rafaqat, N. Ali, C. Torres, and B. Rittmann, "Recent progress in treatment of dyes wastewater using microbial-electro-Fenton technology," *RSC Advances*, vol. 12, no. 27, pp. 17104–17137, 2022, doi: 10.1039/D2RA01831D.

[3] R. Al-Tohamy *et al.*, "A critical review on the treatment of dye-containing wastewater: Ecotoxicological and health concerns of textile dyes and possible remediation approaches for environmental safety," *Ecotoxicology and Environmental Safety*, vol. 231, p. 113160, Feb. 2022, doi: 10.1016/j.ecoenv.2021.113160.

[4] S.-H. Thor *et al.*, "Discovering the roles of electrode distance and configuration in dye degradation and electricity generation in photocatalytic fuel cell integrated electro-Fenton process," *Separation and Purification Technology*, vol. 278, p. 119652, Dec. 2021, doi: 10.1016/j.seppur.2021.119652.

[5] X. Li *et al.*, "Challenges of photocatalysis and their coping strategies," *Chem Catalysis*, vol. 2, no. 6, pp. 1315–1345, Jun. 2022, doi: 10.1016/j.checat.2022.04.007.

[6] J. Safaei *et al.*, "Facile fabrication of graphitic carbon nitride, (g-C_3N_4) thin film," *Journal of Alloys and Compounds*, vol. 769, pp. 130–135, Nov. 2018, doi: 10.1016/j.jallcom.2018.07.337.

[7] A. Dandia, S. L. Gupta, P. Saini, R. Sharma, S. Meena, and V. Parewa, "Structure couture and appraisal of catalytic activity of carbon nitride (g-C_3N_4) based materials towards sustainability," *Current Research in Green and Sustainable Chemistry*, vol. 3, p. 100039, Jun. 2020, doi: 10.1016/j.crgsc.2020.100039.

[8] J. Qin *et al.*, "Direct growth of uniform carbon nitride layers with extended optical absorption towards efficient water-splitting photoanodes," *Nature Communications*, vol. 11, no. 1, p. 4701, Sep. 2020, doi: 10.1038/s41467-020-18535-0.

[9] D. Bhanderi, P. Lakhani, and C. K. Modi, "Graphitic carbon nitride (g-C_3N_4) as an emerging photocatalyst for sustainable environmental applications: a comprehensive review," *RSC Sustainability*, vol. 2, no. 2, pp. 265–287, 2024, doi: 10.1039/D3SU00382E.

[10] J. Xi, H. Li, J. Xi, S. Tan, J. Zheng, and Z. Tan, "Preparation of high porosity biochar materials by template method: a review," *Environmental Science and Pollution Research*, vol. 27, no. 17, pp. 20675–20684, Jun. 2020, doi: 10.1007/s11356-020-08593-8.

[11] I. J. Budiarso, V. A. Dabur, R. Rachmantyo, H. Judawisastra, C. Hu, and A. Wibowo, "Carbon nitride- and graphene-based materials for the photocatalytic degradation of emerging water pollutants," *Materials Advances*, vol. 5, no. 7, pp. 2668–2688, 2024, doi: 10.1039/D3MA01078C.

[12] M. Norek, "Approaches to enhance UV light emission in ZnO nanomaterials," *Current Applied Physics*, vol. 19, no. 8, pp. 867–883, Aug. 2019, doi: 10.1016/j.cap.2019.05.006.

[13] A. Kołodziejczak-Radzimska and T. Jesionowski, "Zinc Oxide—From Synthesis to Application: A Review," *Materials*, vol. 7, no. 4, pp. 2833–2881, Apr. 2014, doi: 10.3390/ma7042833.

[14] M. H. Suhag, A. Khatun, I. Tateishi, M. Furukawa, H. Katsumata, and S. Kaneco, "One-Step Fabrication of the ZnO/g-C_3N_4 Composite for Visible Light-Responsive Photocatalytic Degradation of Bisphenol E in Aqueous Solution," *ACS Omega*, vol. 8, no. 13, pp. 11824–11836, Apr. 2023, doi: 10.1021/acsomega.2c06678.

[15] L. Jurado *et al.*, "Highly dispersed Rh single atoms over graphitic carbon nitride as a robust catalyst for the hydroformylation reaction," *Catalysis Science & Technology*, vol. 13, no. 5, pp. 1425–1436, 2023, doi: 10.1039/D2CY02094G.

[16] D. R. Paul, S. Gautam, P. Panchal, S. P. Nehra, P. Choudhary, and A. Sharma, "ZnO-Modified g-C_3N_4 : A Potential Photocatalyst for Environmental Application," *ACS Omega*, vol. 5, no. 8, pp. 3828–3838, Mar. 2020, doi: 10.1021/acsomega.9b02688.

[17] Q. Wang, A. Chen, X. Wang, J. Zhang, J. Yang, and X. Li, "Fe-species-loaded graphitic carbon nitride with enhanced photocatalytic performance under visible-light irradiation," *Journal of Molecular Catalysis A: Chemical*, vol. 420, pp. 159–166, Aug. 2016, doi: 10.1016/j.molcata.2016.04.020.

[18] X. Guo, J. Duan, C. Li, Z. Zhang, and W. Wang, "Highly efficient Z-scheme g-C_3N_4/ZnO photocatalysts constructed by co-melting-recrystallizing mixed precursors for wastewater treatment," *Journal of Materials Science*, vol. 55, no. 5, pp. 2018–2031, Feb. 2020, doi: 10.1007/s10853-019-04097-0.

[19] A. A. Khan *et al.*, "Preparation and characterization of sulphur and zinc oxide Co-doped graphitic carbon nitride for photo-assisted removal of Safranin-O dye," *RSC Advances*, vol. 14, no. 13, pp. 8871–8884, 2024, doi: 10.1039/D3RA07247A.

[20] N. Li *et al.*, "Z-scheme 2D/3D g-C_3N_4@ZnO with enhanced photocatalytic activity for cephalexin oxidation under solar light," *Chemical Engineering Journal*, vol. 352, pp. 412–422, Nov. 2018, doi: 10.1016/j.cej.2018.07.038.

[21] P. L. Meena, K. Poswal, A. K. Surela, and J. K. Saini, "Synthesis of graphitic carbon nitride/zinc oxide (g-C_3N_4/ZnO) hybrid nanostructures and investigation of the effect of ZnO on the photodegradation activity of g-C_3N_4 against the brilliant cresyl blue (BCB) dye under visible light irradiation," *Advanced Composites and Hybrid Materials Mater*, vol. 6, no. 1, p. 16, Feb. 2023, doi: 10.1007/s42114-022-00577-1.

[22] P. Choudhary, A. Bahuguna, A. Kumar, S. S. Dhankhar, C. M. Nagaraja, and V. Krishnan, "Oxidized graphitic carbon nitride as a sustainable metal-free catalyst for hydrogen transfer reactions under mild conditions," *Green Chemistry*, vol. 22, no. 15, pp. 5084–5095, 2020, doi: 10.1039/D0GC01123A.

[23] J. Fu, Q. Xu, J. Low, C. Jiang, and J. Yu, "Ultrathin 2D/2D WO_3/g-C_3N_4 step-scheme H_2-production photo catalyst," *Applied Catalysis B: Environmental*, vol. 243, pp. 556–565, Apr. 2019, doi: 10.1016/j.apcatb.2018.11.011.

[24] P. Tang, S. Eckstein, B. Ji, B. Pan, and G. Sun, "Hierarchical porous nanofibrous aerogels with wide-distributed pore sizes for instantaneous organophosphorus pesticides decontamination-and-fluorescence sensing," *Chemical Engineering Journal*, vol. 450, p. 138183, Dec. 2022, doi: 10.1016/j.cej.2022.138183.

[25] M. S. Akple, T. Ishigaki, and P. Madhusudan, "Bio-inspired honeycomb-like graphitic carbon nitride for enhanced visible light photocatalytic CO_2 reduction activity," *Environmental Science and Pollution Research*, vol. 27, no. 18, pp. 22604–22618, Jun. 2020, doi: 10.1007/s11356-020-08804-2.

[26] S. V. P. Vattikuti, P. A. K. Reddy, J. Shim, and C. Byon, "Visible-Light-Driven Photocatalytic Activity of SnO_2 –ZnO Quantum Dots Anchored on g-C_3N_4 Nanosheets for Photocatalytic Pollutant Degradation and H_2 Production," *ACS Omega*, vol. 3, no. 7, pp. 7587–7602, Jul. 2018, doi: 10.1021/acsomega.8b00471.

[27] M. Yousefi, S. Villar-Rodil, J. I. Paredes, and A. Z. Moshfegh, "Oxidized graphitic carbon nitride nanosheets as an effective adsorbent for organic dyes and tetracycline for water remediation," *Journal of Alloys and Compounds*, vol. 809, p. 151783, Nov. 2019, doi: 10.1016/j.jallcom.2019.151783.

[28] Y. Sun *et al.*, "Improving g-C_3N_4 photocatalysis for NO_x removal by Ag nanoparticles decoration," *Applied Surface Science*, vol. 358, pp. 356–362, Dec. 2015, doi:

10.1016/j.apsusc.2015.07.071.

[29] S. Suganthi, S. Vignesh, J. K. Sundar, S. A. Alqarni, S. Pandiaraj, and T. H. Oh, "Cobalt oxide coupled with graphitic carbon nitride composite heterojunction for efficient Z-scheme photocatalytic environmental pollutants degradation performance," *Environmental Research*, vol. 235, p. 116574, Oct. 2023, doi: 10.1016/j.envres.2023.116574.

[30] A. H. Navidpour *et al.*, "Zinc oxide@citric acid-modified graphitic carbon nitride nanocomposites for adsorption and photocatalytic degradation of perfluorooctanoic acid," *Advanced Composites and Hybrid Materials*, vol. 7, no. 2, p. 53, Apr. 2024, doi: 10.1007/s42114-024-00867-w.

[31] S. Hu, F. Li, Z. Fan, F. Wang, Y. Zhao, and Z. Lv, "Band gap-tunable potassium doped graphitic carbon nitride with enhanced mineralization ability," *Dalton Transactions*, vol. 44, no. 3, pp. 1084–1092, 2015, doi: 10.1039/C4DT02658F.

[32] G. Liu, Z. Zhang, M. Lv, H. Wang, D. Chen, and Y. Feng, "Photodegradation performance and transformation mechanisms of sulfamethoxazole by porous g-C_3N_4 modified with ammonia bicarbonate," *Separation and Purification Technology*, vol. 235, p. 116172, Mar. 2020, doi: 10.1016/j.seppur.2019.116172.

[33] B. Singh *et al.*, "Nanostructured BN–TiO_2 composite with ultra-high photocatalytic activity," *New Journal of Chemistry*, vol. 41, no. 20, pp. 11640–11646, 2017, doi: 10.1039/C7NJ02509B.

[34] L. Korala, J. R. Germain, E. Chen, I. R. Pala, D. Li, and S. L. Brock, "CdS aerogels as efficient photocatalysts for degradation of organic dyes under visible light irradiation," *Inorganic Chemistry Frontiers*, vol. 4, no. 9, pp. 1451–1457, 2017, doi: 10.1039/C7QI00140A.

[35] R. M. Mohamed, A. A. Ismail, and M. Alhaddad, "A novel design of porous Cr_2O_3@ZnO nanocomposites as highly efficient photocatalyst toward degradation of antibiotics: A case study of ciprofloxacin," *Separation and Purification Technology*, vol. 266, p. 118588, Jul. 2021, doi: 10.1016/j.seppur.2021. 118588.

[36] S.-L. Lee *et al.*, "Exploring the relationship between molecular structure of dyes and light sources for photodegradation and electricity generation in photocatalytic fuel cell," *Chemosphere*, vol. 209, pp. 935–943, Oct. 2018, doi: 10.1016/j.chemosphere. 2018.06.157.

[37] S. John, W. Nogala, B. Gupta, and S. Singh, "Synergy of photocatalysis and fuel cells: A chronological review on efficient designs, potential materials and emerging applications," *Frontiers in Chemistry*, vol. 10, Nov. 2022, doi: 10.3389/fchem.2022.1038221.

[38] J.-X. Sun *et al.*, "Fabrication of composite photocatalyst g-C_3N_4–ZnO and enhancement of photocatalytic activity under visible light," *Dalton Transactions*, vol. 41, no. 22, p. 6756, 2012, doi: 10.1039/c2dt12474b.

[39] X. Zhao, Y. Zhang, P. Wen, G. Xu, D. Ma, and P. Qiu, "NH_2-MIL-125(Ti)/TiO_2 composites as superior visible-light photocatalysts for selective oxidation of cyclohexane," *Molecular Catalysis*, vol. 452, pp. 175–183, Jun. 2018, doi: 10.1016/j.mcat.2018.04.004.

[40] B. Weng, M.-Y. Qi, C. Han, Z.-R. Tang, and Y.-J. Xu, "Photocorrosion Inhibition of Semiconductor-Based Photocatalysts: Basic Principle, Current Development, and Future Perspective," *ACS Catalysis*, vol. 9, no. 5, pp. 4642–4687, May 2019, doi: 10.1021/ acscatal.9b00313.

[41] F. Dong, Y. Li, Z. Wang, and W.-K. Ho, "Enhanced visible light photocatalytic activity and oxidation ability of porous graphene-like g-C_3N_4 nanosheets via thermal exfoliation," *Applied Surface Science*, vol. 358, pp. 393–403, Dec. 2015, doi: 10.1016/j.apsusc.2015. 04.034.

[42] P.-Y. Kuang *et al.*, "g-C_3N_4 decorated ZnO nanorod arrays for enhanced photoelectrocatalytic performance," *Applied Surface Science*, vol. 358, pp. 296–303, Dec. 2015, doi: 10.1016/j.apsusc.2015. 08.066.